Article

Wavenumber-4 Structure in COSMIC-2 Observations: Vertical Plane Perspective

Lalit Mohan Joshi [1,*] **, Lung-Chih Tsai** [2] **and Shin-Yi Su** [2]

1   GPS Science and Application Research Center, National Central University, Taoyuan City 320317, Taiwan
2   Center for Space and Remote Sensing Research, National Central University, Taoyuan City 320317, Taiwan;
     lctsai@csrsr.ncu.edu.tw (L.-C.T.); sysu@csrsr.ncu.edu.tw (S.-Y.S.)
*   Correspondence: lmjoshinarl@gmail.com or lmjoshi@csrsr.ncu.edu.tw

Abstract: High-rate radio occultation (RO) in COSMIC-2 (FORMOSAT7) enables us to investigate the finer details of the ionosphere owing to the measurements being made at a significantly high spatiotemporal resolution, which was unthinkable a decade ago. In the vertical plane, local-time ionospheric wavenumber-4 (WN4) structures display tilted phase-fronts over the equatorial ionization anomaly (EIA) belt. The longitudinal extent of a tilted WN4 phase-front approximates the zonal wavelength of nonmigrating DE3 tide in the local-time frame of reference, i.e., $\sim 90^0$. The WN4-filtered (residual) component indicates a greater tilt (when visible), with a larger longitudinal extent of a wavenumber structure in the vertical plane. The WN4 structure over the EIA crest region is found to be out of phase (in phase) with respect to that over the EIA trough region during daytime (nighttime), which also depended on the altitude under consideration. Intriguingly, above 400 km, the WN4 structures in the EIA crest and trough regions are seen to be in phase with each other at all local times. The phenomenon of the "longitudinal co-location" of WN4 over the EIA crest and trough regions at altitudes above ~400 km at all local times remains unexplained. Results also highlight that the formation of WN4 is governed by a complex interplay of direct forcing of nonmigrating tides and the zonal electric field whose characteristics within the EIA belt vary drastically with latitude and altitude under consideration.

Keywords: wavenumber-4 structure; nonmigrating tides; COSMIC-2 radio occultation

1. Introduction

Longitudinal modulation of ionospheric plasma density driven by nonmigrating tides originating in the lower atmosphere has been extensively studied in the last ~2 decades. Four-peaked longitudinal structure (wavenumber-4 structure) in local-time ionospheric UV emissions was first reported by Sagawa et al. [1], and further investigation by Immel et al. [2] suggested the wavenumber-4 structure be associated with the nonmigrating diurnal eastward-propagating tide having zonal wavenumber 3, commonly referred to as DE3 (diurnal, eastward propagating, zonal wavenumber 3; tidal terminology is discussed in the subsequent paragraph). England et al. [3] analyzed equatorial electrojet (EEJ) intensity and found a prominent presence of four-peaked longitudinal structures in it, signifying that the local-time zonal electric field (or vertical EXB drift) also has a wavenumber-4 structure. A detailed investigation of nonmigrating tidal signature in the EEJ was performed by Lühr et al. [4]. Wavenumber-4 structure was also found to exist in the vertical plasma drift [5]. Over time, several reports have been published on longitudinal wavenumber 4 and other modulations of the ionospheric density in the equatorial ionization anomaly belt [6–11]. All these reports indicate a predominant relation between ionospheric wavenumber-4 structure and nonmigrating tides, particularly DE3. The neutral winds associated with the nonmigrating tides can modulate the background zonal polarization electric field in the ionosphere. The general explanation is that the nonmigrating tides alter the E-region electric field which maps to the ionospheric F region and

results in the longitudinal variations of the equatorial ionization anomaly (EIA). However, Maute et al. [12] suggested that the longitudinal variation of vertical plasma drift is driven by neutral winds in both the E and F regions. They also indicated that the relative importance of E- and F-region winds in the vertical plasma drift depends on local time as well as solar activity. It must be mentioned that the impact of nonmigrating tides on the ionosphere is generally studied in the local-time frame of reference, i.e., local-time ionosphere. Longitudinal variation of the ionosphere at a particular universal time would be overcast by the most significant variation caused by photoionization and recombination. Consequently, the DE3 tide having a wavenumber 3 in UT frame of reference manifests in the form of a four-peaked structure in the local-time frame of reference.

Nonmigrating DE2 and DE3 tides are mainly driven by latent heat release from tropospheric deep convection over the tropics [13,14]. In tidal terminology, D(S) and E(W) refer to diurnal (semidiurnal) and east (west), respectively. The number that follows indicates the zonal wavenumber. These reports also indicate that the DE3 amplitude in terms of temperature and wind maximizes at ~100 km altitude. TIMED observations have revealed the presence of DE2 and DE3 tides in the MLT (mesosphere and lower thermosphere) region [15–18]. However, DE2/DE3 signatures in neutral wind and density have been detected at 400 km altitude by the CHAMP satellite [19,20]. The E region is the most efficient altitude region for ion-neutral coupling, and thus, the wavenumber-4 structure in the EIA is considered to be driven by the zonal electric field produced in the E region. Jin et al. [21], based on simulation, reported that the zonal electric field responsible for the wavenumber-4 structure in the EIA during the daytime (nighttime) is produced by the neutral wind at E-region (F-region) altitude. Lei et al. [22], based on TIME-GCM simulations, reported that the zonal wavenumber-4 structures in the thermospheric density are formed as a result of the direct response of the upper thermosphere to the DE3 and semidiurnal eastward wavenumber 2 (SE2) nonmigrating tides. They, however, also reported that the wavenumber-4 structure in the EIA is formed due to the modulation of wind dynamo by nonmigrating tides. Pancheva et al. [23], based on COSMIC RO measurement, reported for the first time the existence of tilted phase fronts in the wavenumber structure. Tilted phase fronts were mainly observed in the height region of 200–300 km, while above that, the phase fronts were vertical, mainly attributed to the "fountain effect" [24].

Over the last few decades, the ionospheric radio occultation (RO) technique has emerged as one of the most powerful tools for deriving spatiotemporal variability in the vertical profile of electron density and irregularity. The recently launched COSMIC-2 mission provides ionospheric observations at unprecedented spatial and temporal scale with ~3500–4000 profiles in a day. Previous COSMIC data have already been utilized in the study of ionospheric wavenumber structures. Lin et al. [6] were the first to present longitudinal four-peaked structures in the local-time electron density obtained from COSMIC RO. Other investigations based on COSMIC RO have also studied ionospheric wavenumber structures (e.g., [10,11]). Recently, Niu [25] presented wavenumber-4 in E-region scintillation in COSMIC data and its relation with nonmigrating DE3 tide. Pioneering studies on wavenumber structures based on IMAGE-FUV observations [1,2], as well as investigations based on CHAMP electron density measurements [26], reveal two-dimensional local-time longitudinal behavior of the phenomenon. However, the RO technique makes it possible to study the wavenumber structures in the altitude–longitude plane as well. Owing to the high sampling rate of COSMIC-2, statistical characteristics of wavenumber structures can be examined with high spatial and altitudinal resolution. The present study attempts to utilize the COSMIC-2 dataset to understand the characteristics of wavenumber structuring of the ionospheric density.

2. Data and Analysis

COSMIC-2/FORMOSAT-7 is a constellation of six satellites employed to derive electron density profiles in the ionosphere using the Global Navigation Satellite System (GNSS) radio occultation (RO) technique. In order to derive the profile of electron density from oc-

cultation measurement, Abel integral transform algorithms are utilized, which consider the electron density field to be spherically symmetric [27]. The constellation was launched in June 2019 into 24° low-inclination orbits and has been optimally distributed into intended orbits at an altitude of ~550 km. Owing to a low inclination orbit, and ~3500–4000 profiles a day, COSMIC-2 is optimized for low–mid-latitude research. In the present study, electron density profile data were binned into monthly average electron density with a latitudinal, longitudinal, local-time, and height resolution of 2.5^0, 10^0, 1 h, and 5 km, respectively. Such a resolution is good enough to study the local-time longitudinal wavenumber structures in the ionosphere. Figure 1 presents the latitudinal–longitudinal variation of electron density at 302.5 km (300–305 km bin) during 12–13 LT in January to December months. The EIA crest and trough regions appear with a distinct contrast in the plots, unlike in the earlier reports based on previous COSMIC data [6]. Possibly, a higher sampling rate which allows a better spatial resolution and larger data points to derive average values leads to better mapping of ionospheric structures in COSMIC-2. The black curve in these plots indicates the location of the magnetic equator and the white color indicates lack of measurement. Note that the measurement gaps are mostly seen at higher latitudes, which were somewhat reduced after August. This highlights a higher sampling rate closer to the Equator. Figure 1 indicates that the local-time EIA electron density varies longitudinally during 12–13 LT. For example, in September month (Figure 1i), EIA appears to be stronger in the vicinity of -100^0, 0^0, and 100^0 in comparison to longitudes sandwiched between them. In addition, the electron density in the EIA region varies in different months; it is higher in the equinoctial months and lower during the summer months. Temporal and altitudinal characteristics of longitudinal electron density structures based on COSMIC-2 data are presented in the subsequent sections of this paper.
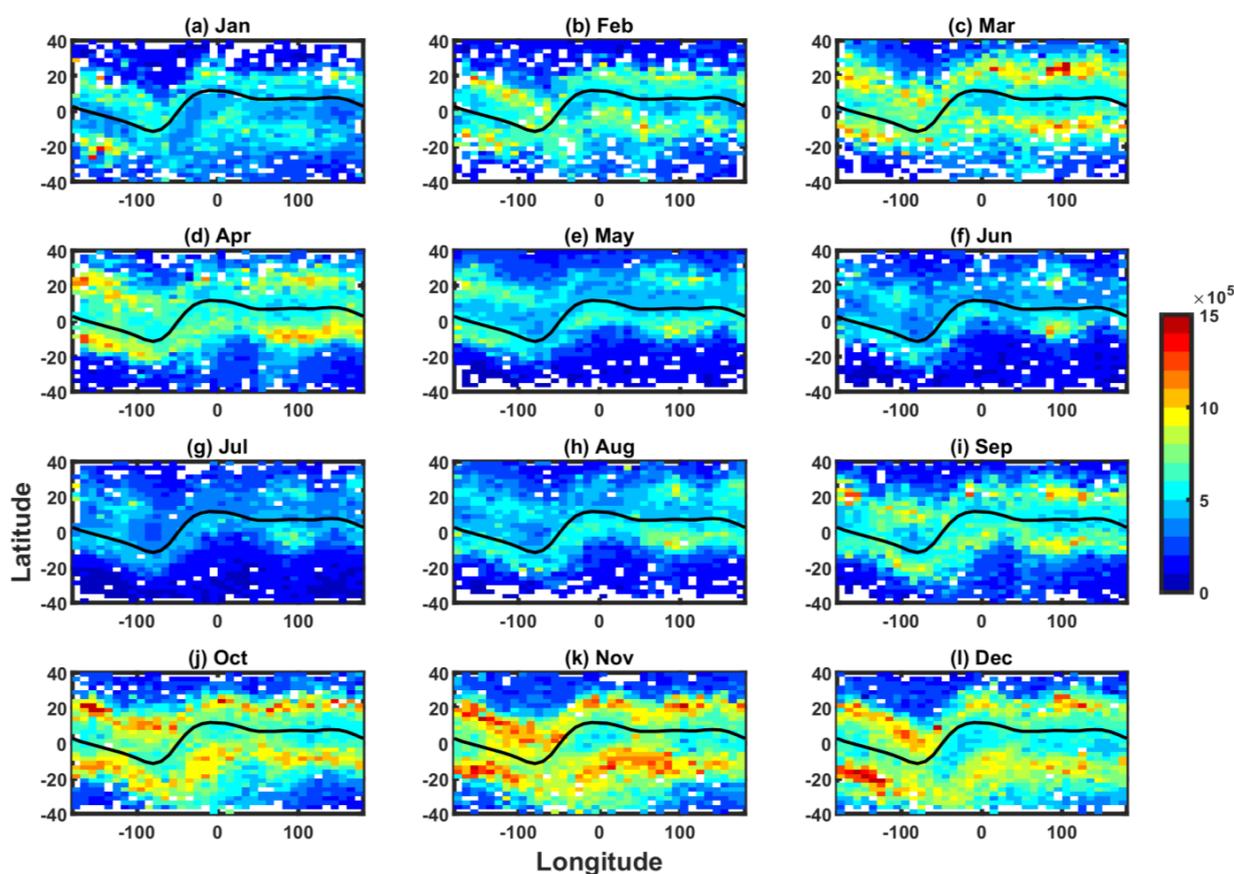

Figure 1. Latitude–longitude maps of electron density at 302.5 km (300–305 km mean) during 12–13 LT based on COSMIC-2 data. (**a–l**) January to December months in 2020. The black curve represents the magnetic equator.

3. Results

3.1. Characteristics of Wavenumber Structures

Nonmigrating tidal signatures in the local-time ionospheric density are evaluated by examining its longitudinal pattern along with local-time progression. Figure 2a shows the local-time longitudinal variability of EIA zone electron density at 302.5 km altitude during September 2020. EIA zone electron density is represented by the average electron density of the belt lying between $\pm 20^0$ geomagnetic latitude. The local-time and longitude resolutions for the analysis are 1 h and 10^0, respectively. In Figure 2a, longitudinal structuring can be seen and the propagation of the structures appears to be predominantly eastward. These structures and their propagation can be better visualized after the zonal mean is removed (e.g., [26]). Figure 2b shows the local-time longitudinal variation of EIA electron density after subtracting the zonal mean electron density. The process of DC removal leaves only the oscillatory component of electron density, resulting in the contrast enhancement of the wavenumber structures. Structures appear to propagate in the eastward direction, with a larger westward-tilted envelope. These longitudinal structures can be seen both during the daytime and the nighttime. However, owing to the diurnal variation of the background electron density with a maximum around 13–15 LT, it is difficult to visualize the time-dependent variation of these structures. Thus, the DC-removed electron density has also been further normalized with respect to peak electron density at that particular local-time epoch. Figure 2c shows the local-time longitudinal variation of the zonal mean removed and normalized EIA electron density. It clearly shows that (1) four peak longitudinal wavenumber-4 (WN4) structures propagate eastward, and (2) the WN4 structures are as prominent during the daytime as during the night.

Figure 2d presents the altitudinal longitudinal variation of EIA density at 12–13 LT during September 2020. It shows the F-region peak to be at ~300–315 km and the longitudinal wavenumber structures to be present at all altitudes. Such structures are better visualized after DC removal. Figure 2e shows the same distribution after subtracting the zonal mean at every altitude bin. Longitudinal structuring is clearly seen. To offset the altitude variation of electron density to reveal the relative impact of wavenumber structuring at different altitudes, zonal mean removed electron density is further normalized with respect to the maximum electron density for each altitude bin. Figure 2f presents the altitudinal longitudinal variation of the zonal mean removed and normalized EIA density. It clearly shows the longitudinal wavenumber structuring to display a similar relative impact at all altitude bins. However, the phase of the wavenumber structuring varies with the altitude. Its implications and possible causative mechanism will be discussed later in the paper. For further analysis in this paper, only zonal mean removed and normalized electron density was used, as it removes temporal/altitudinal variation of electron density (mainly attributable to ionization production/loss), thus highlighting the impact of wavenumber structuring that is commonly attributable to nonmigrating tidal effects.

Ionospheric electron density is impacted by several tidal components, which results in different wavenumbers being present concurrently. The wavenumber-4 structure is the most prominent feature of the nonmigrating tidal forcing. It is commonly attributed to DE3 tidal impact. In the analysis, the WN4 component is filtered from the normalized electron density. Figure 3a shows the unfiltered (total), WN4-filtered, and WN4 components of normalized electron density at 00–01 LT in September 2020. The WN4 component is seen oscillating around the zero level, while the WN4-filtered component appears to be a single sinusoid (wavenumber 1). In simple words, the unfiltered electron density is the total electron density (DC removed + normalized), the WN4 component represents the high-frequency oscillations, and the WN4-filtered component represents the residual after WN4 removal. It must be noted that the WN4-filtered component, as such, does not represent any unambiguous tidal component. It only indicates the residual after removing the WN4 oscillation from the unfiltered (total) electron density. In Figure 2c (00 LT), it is possible to visualize WN4 and lower wavenumber components; however, after filtering, their characteristics can be better studied. Figure 3b,c show the local-time

longitudinal variability of the WN4-filtered component and WN4 components, respectively. The WN4 component shows eastward propagation. A phase-transition node is seen in the WN4 component at ~06 LT. Earlier investigations hypothesized the presence of two phase-transition nodes, at 06 LT and 18 LT [21]. Those investigations considered the WN4 structures to be driven by similar wavenumbers in the zonal electric field, with the electric field during daytime (nighttime) originating in the E region (F region). Thus, two phase-transition nodes are generally expected, one at dawn and the other at dusk. However, Figure 3c does not seem to indicate any distinct phase transition at dusk. It more closely resembles a natural and direct propagation of DE3.
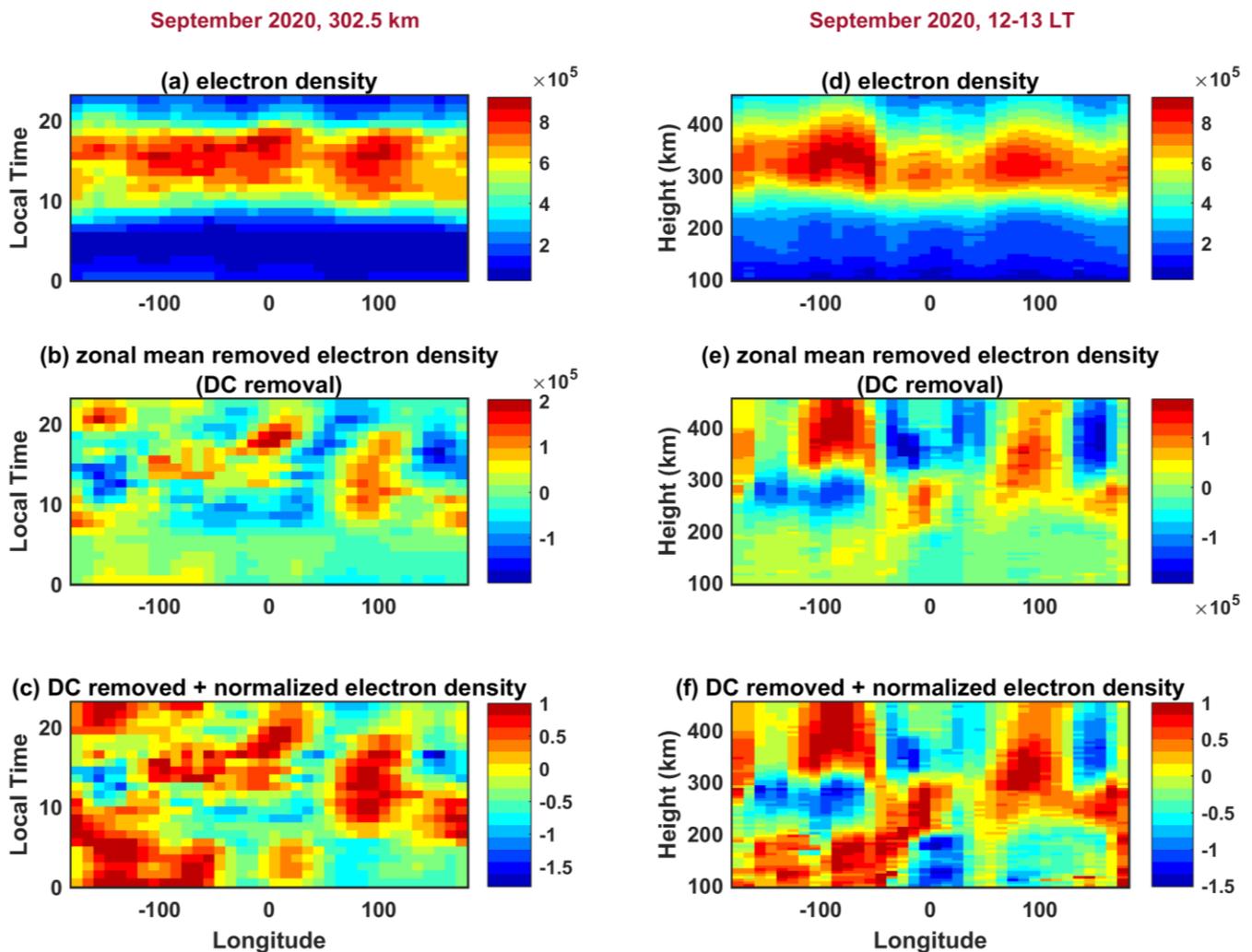

Figure 2. Panels (**a**–**c**) present local-time longitude variation of electron density, DC-removed electron density, and DC-removed + normalized electron density, respectively, at 302.5 km altitude (300–305 km mean) in September 2020. Electron density here represents the average electron density of the belt lying within ±200 of the magnetic equator. Panels (**d**–**f**) present the variation of these electron densities in the altitude–longitude plane during 12–13 LT.

(a) Electron density 00LT September (zonal mean removed +normalized)

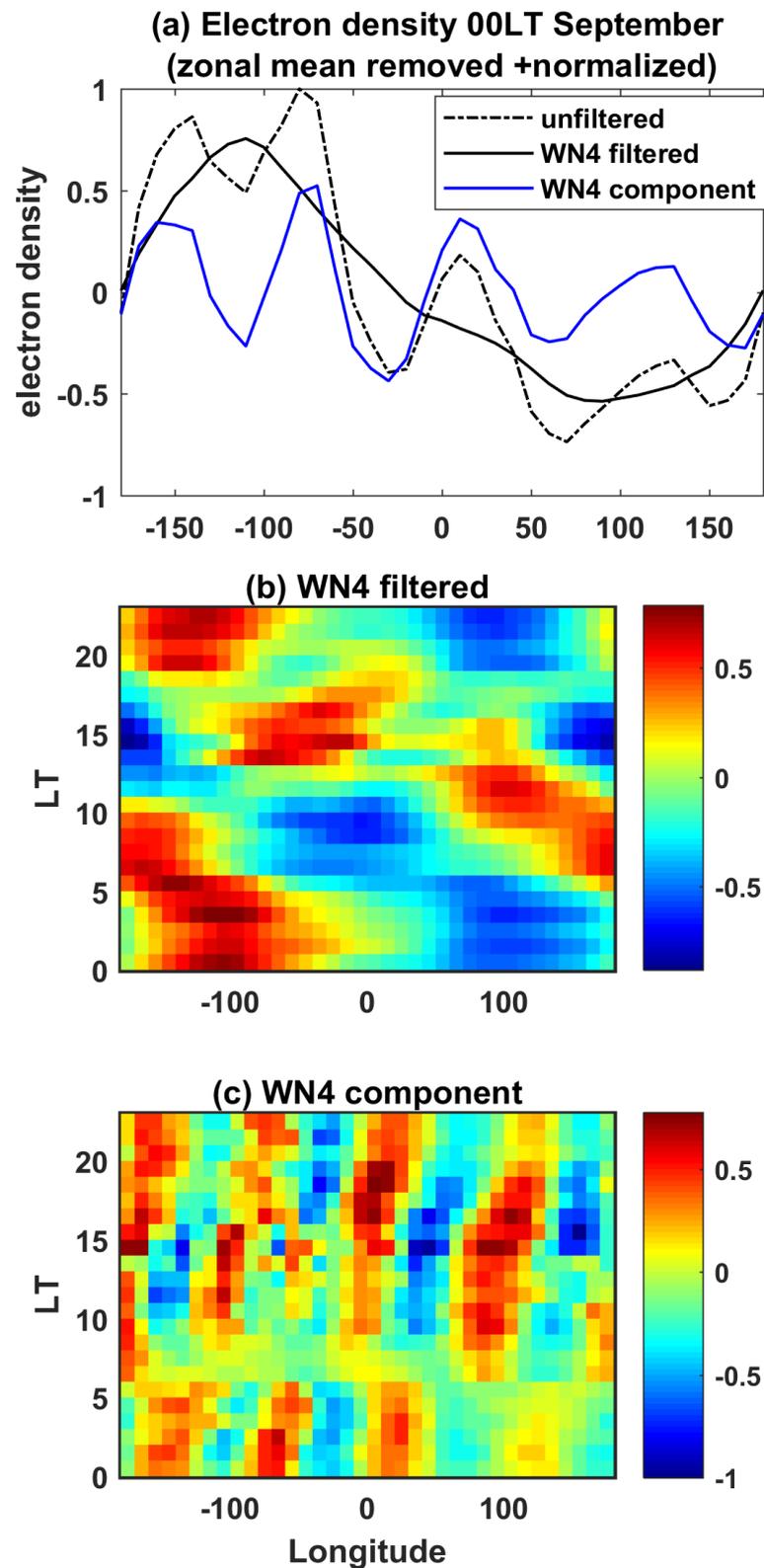**(b) WN4 filtered**

(c) WN4 component

Figure 3. DC-removed + normalized electron density at 302.5 km altitude split into WN4-filtered (residual) and WN4 component. Panel (**a**) presents unfiltered, WN4-filtered, and WN4 components at 00 LT in September 2020. Panels (**b**,**c**) present the local-time variation of the WN4-filtered component and WN4 component, respectively. Note the eastward propagation in the WN4 component which can be generally attributed to DE3 propagation.

3.2. Characteristics of Wavenumber Structures in the Vertical Plane

Nonmigrating tidal forcing in the ionospheric density can create local-time longitudinal structures. Such wavenumber structures can influence all ionospheric heights. Thus, the variation of wavenumber structure with altitude needs to be studied. Unlike in the in situ or columnar measurement from satellite platforms such as CHAMP and IMAGE, which only provide measurement either at satellite altitude or columnar (e.g., [1,26]), the RO profile inversion technique can be applied to study wavenumber structures at all ionospheric altitudes. Figure 4 presents the hourly variation of the WN4-filtered component in the vertical plane in September 2020. Here, panels a–x indicate the hourly picture of the WN4-filtered component for the entire 24 h period. Tilt in the phase front of the wavenumber structuring can often be seen. At different time epochs, tilt is either westward, eastward, or not clearly defined. Such phase front tilts can be indicative of a direct vertical propagation of neutral atmospheric tides and waves, which have tilted phase fronts.
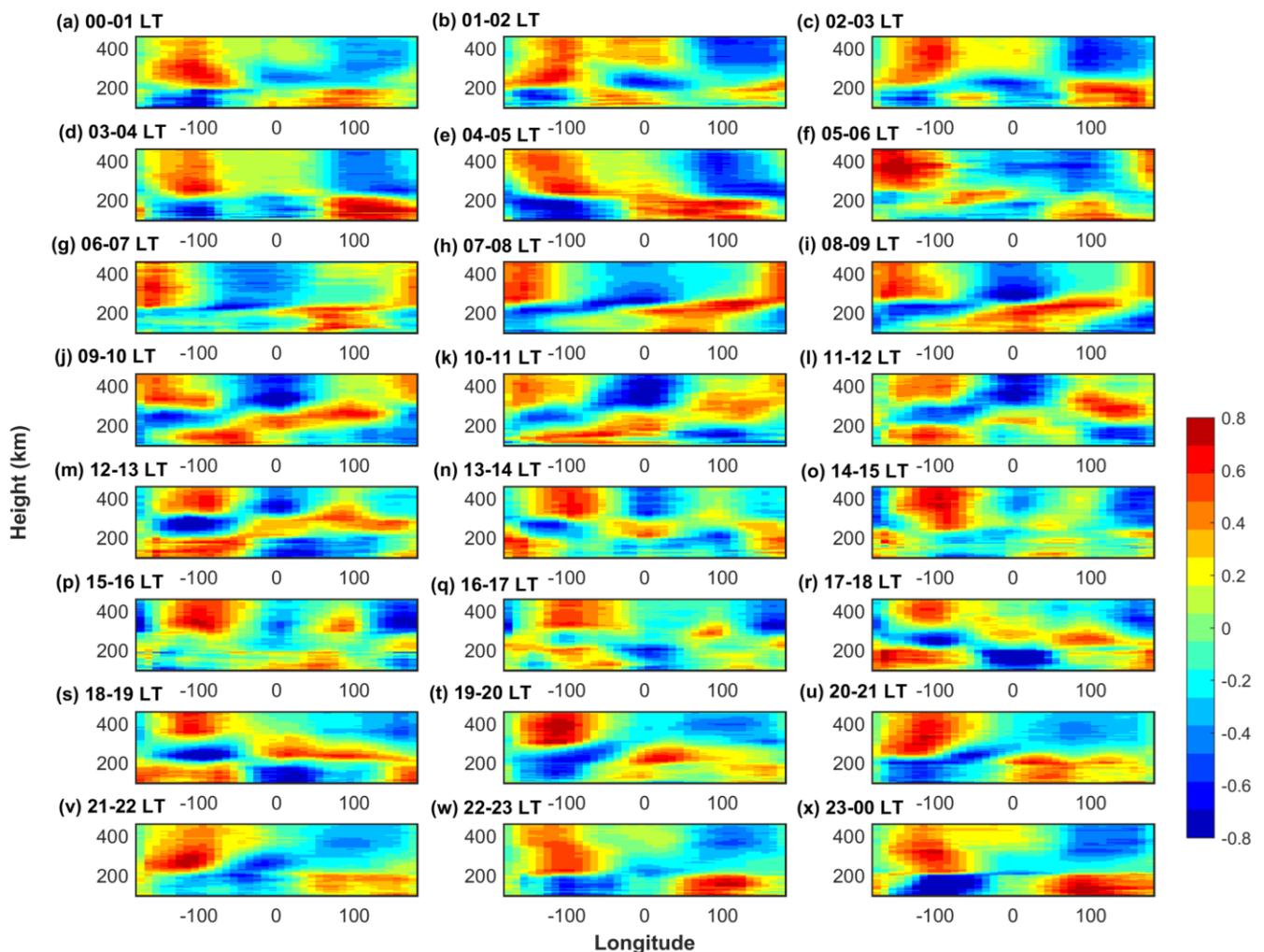

Figure 4. Hourly maps of altitude–longitude variation of WN4-filtered (residual) component of normalized electron density for September 2020. Panels (**a**–**x**) represent hourly epoch from 00–01 LT to 23–00 LT.

Figure 5 presents the hourly variation of the WN4 component in the vertical plane in the month of September. Here, panels a–x indicate the hourly picture of the WN4 component for the entire 24 h period. The tilt in the phase front of the WN4 component in the vertical plane can be clearly seen. However, the tilt is more often seen at altitudes below ~300–350 km. Above that altitude, the phase fronts are mostly vertical. Plausibly, the direct

tidal forcing responsible for the formation of the WN4 structure remains effective at lower heights, while above that, the WN4 is driven by the large-scale zonal electric field. This is just a possible explanation; however, its actual justification would require the matching observation of tides and electric fields in the vertical plane.
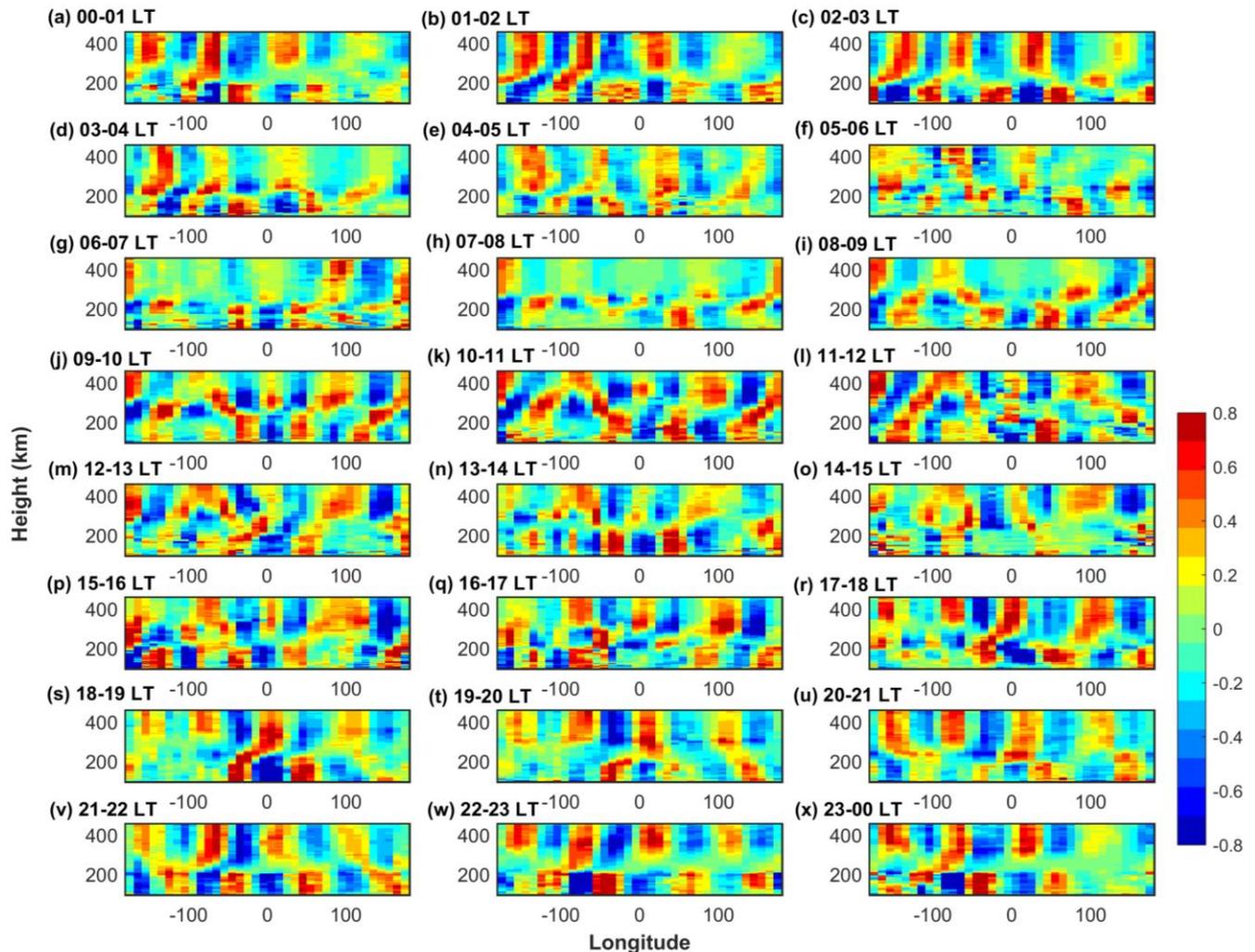

Figure 5. Hourly maps of altitude–longitude variation of WN4 component of normalized electron density for September 2020. Panels (**a**–**x**) represent hourly epoch from 00–01 LT to 23–00 LT.

3.3. Propagation of WN4 Structure over EIA Crest/Trough

So far, the zonal wavenumber structure has been presented as the aggregate entity for electron density averaged over the entire EIA belt. Such a description is fair enough to resolve the broad propagation characteristics of wavenumber structures. However, the characteristics of the wavenumber structure can have significant variations within the EIA belt. Figure 6 presents the local-time progression of WN4 and WN4-filtered components of normalized electron density at 350 km altitude over the EIA crest/trough regions in September 2020. In Figure 6, panels (a) and (b) indicate the WN4 propagation over the EIA crest and trough regions, respectively. Panels (c) and (d) indicate the local-time behavior of the WN4-filtered component over the EIA crest and trough regions, respectively. Note that the electron density of the EIA trough region has been identified as the average electron density in the region lying within $\pm 5^0$ of the geomagnetic equator, while the electron density of the EIA crest region is the average electron density in the region lying within 10^0–20^0 geomagnetic latitude. Propagation characteristics of the WN4-filtered component appear to be similar over the EIA trough and crest regions. However, the local-time progression of

the WN4 structure is not identical over EIA trough and crest regions. During the nighttime, the WN4 component over the EIA trough and crest is longitudinally collocated. During the daytime, however, there appears to be a longitudinal phase differential between the two. The daytime WN4 propagation over the EIA trough region (as presented in Figure 6b) can be characterized as having a "c-shaped" propagation, indicated by the black curves in Figure 6b.
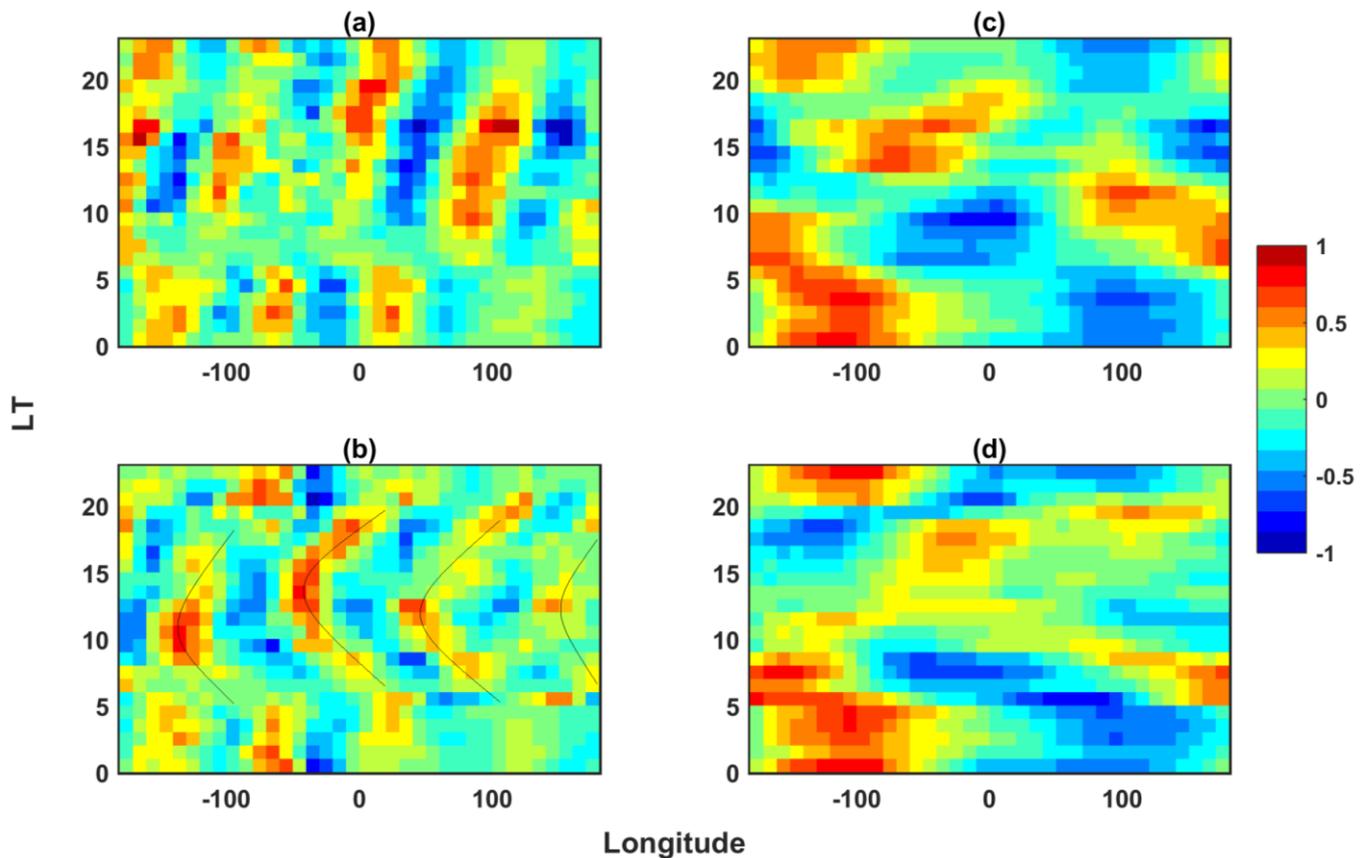

Figure 6. (**a**,**b**) Local-time variation of WN4 component of normalized electron density at 302.5 km altitude over the EIA crest (panel **a**) and trough (panel **b**) regions. (**c**,**d**) Local-time variation of WN4-filtered (residual) component of normalized electron density at 302.5 km altitude over the EIA crest (panel **c**) and trough (panel **d**) regions.

Characteristics of the WN4 component in the vertical plane over the EIA crest and trough were also examined. Figure 7a,b present the WN4 altitude–longitude contour map of normalized electron density over the EIA crest/trough regions during the nighttime (00–01 UT) and daytime (12–13 UT), respectively. The top and bottom panels indicate the EIA crest and trough regions, respectively. It is interesting to see that the features of WN4 in the vertical plane corresponding to the EIA trough and crest region are broadly identical during the nighttime. In other words, WN4 peaks are longitudinally collocated over crest and trough regions. However, during the daytime, the features of WN4 in the vertical plane over the EIA crest and trough are not broadly identical. Interestingly, above ~400 km, WN4 peaks are longitudinally collocated over the EIA crest and trough regions, even during the daytime. Below 400 km, however, the WN4 peaks are not longitudinally collocated over the EIA crest and trough regions.
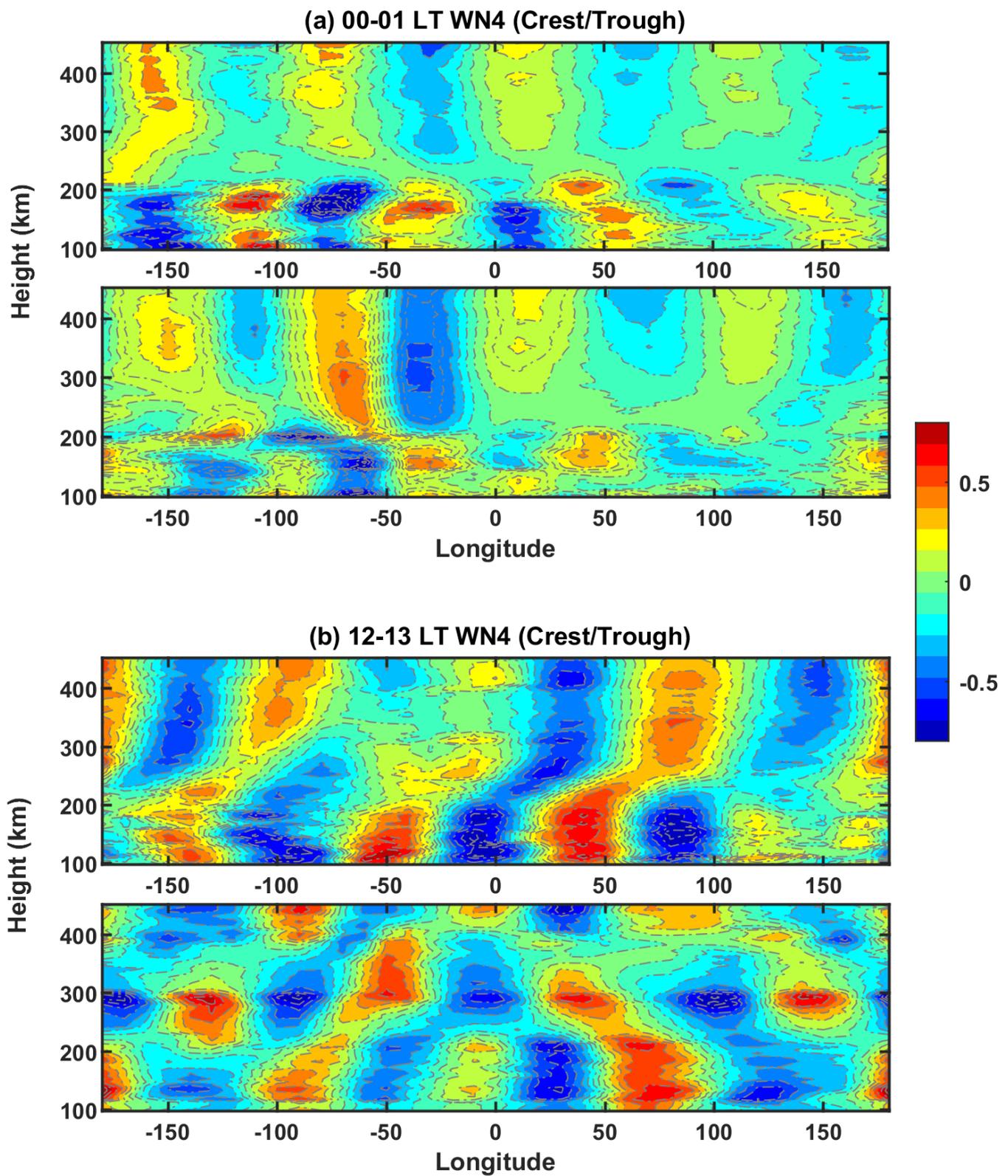
Figure 7. (**a**) Nighttime (local time 00–01) contour of normalized electron density in the vertical plane over the EIA crest and trough regions are presented in the top and bottom subpanels, respectively. (**b**) Daytime (local time 12–13) contour of normalized electron density in the vertical plane over the EIA crest and trough regions are presented in the top and bottom subpanels, respectively.

WN4 structures and longitudinal phase differential over EIA trough and crest regions at various altitude levels were also examined. Figure 8a–f present the WN4 component in normalized electron density over the EIA trough/crest region at six different altitude levels. In these plots, the WN4 component over the EIA crest and trough regions are indicated with red and blue color, respectively. At 200 and 250 km, the WN4 component over the EIA trough/crest region displays an out-of-phase relationship at all local times. At 300 km and upwards, the nighttime WN4 component appears in phase over EIA trough and crest regions. Above 400 km, the WN4 component over the EIA trough and crest displays in-phase relation at all local times. To quantify the longitudinal phase differential, the EIA trough and crest WN4 component was further subjected to lag correlation analysis. The phase difference (magnitude) was calculated for every altitude bin (5 km height resolution) and was averaged for every 50 km height region (10 values). Figure 9a–e present the WN4 longitudinal difference between the EIA crest and trough at five different height bands within 200 to 450 km altitude. Different colors were used to indicate different months of the year, with the x and y axes representing the longitudinal phase difference between the WN4 component over the EIA crest and trough regions, and local time, respectively. From this analysis, it can be inferred that the WN4 in the EIA crest and trough has a general out-of-phase relationship during the daytime when the fountain effect is active. In Figure 9e, it is intriguing to see that the WN4 component in the EIA crest and trough has an in-phase relationship at all local times in 400–450 km (except in December). Less longitudinal difference seen in Figure 8e signifies that in the height region 400–450 km, WN4 peaks over EIA crest and trough are longitudinally collocated.
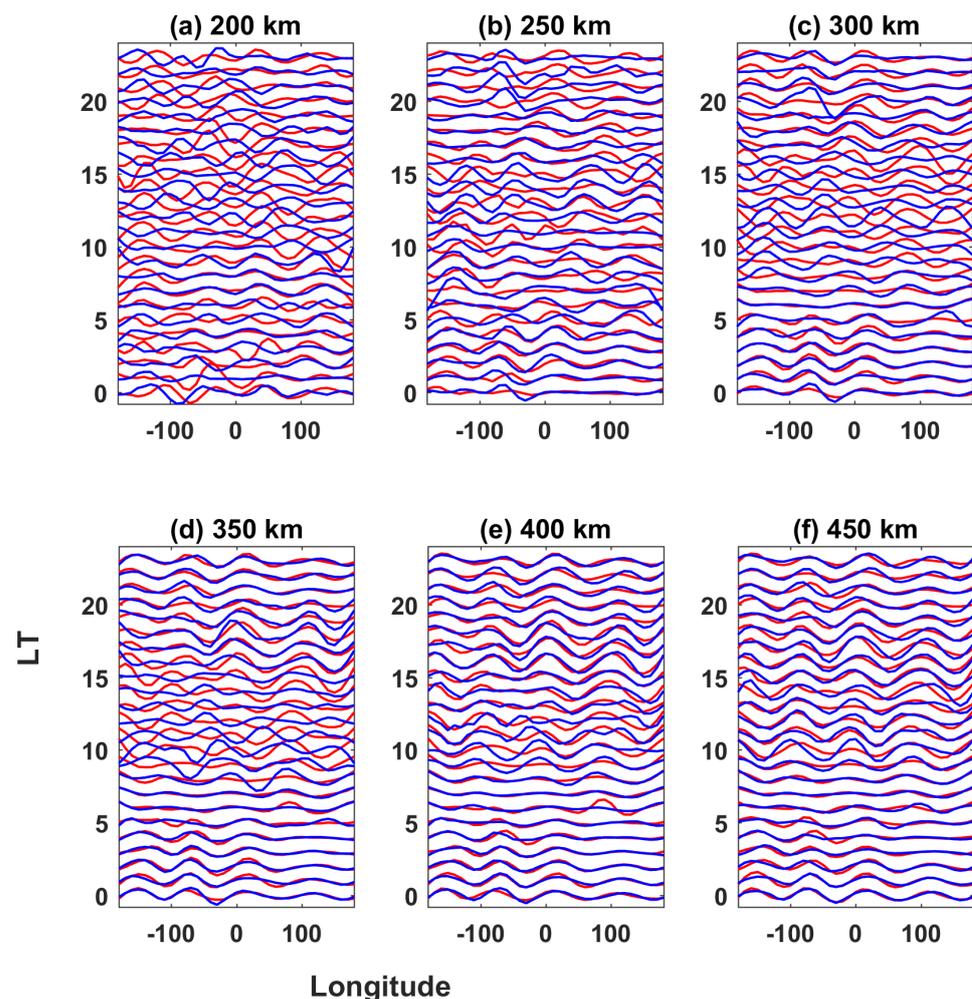

Figure 8. (**a**–**f**) Local-time variation of WN4 component related to EIA crest (red) and trough (blue) regions at 6 different height levels.

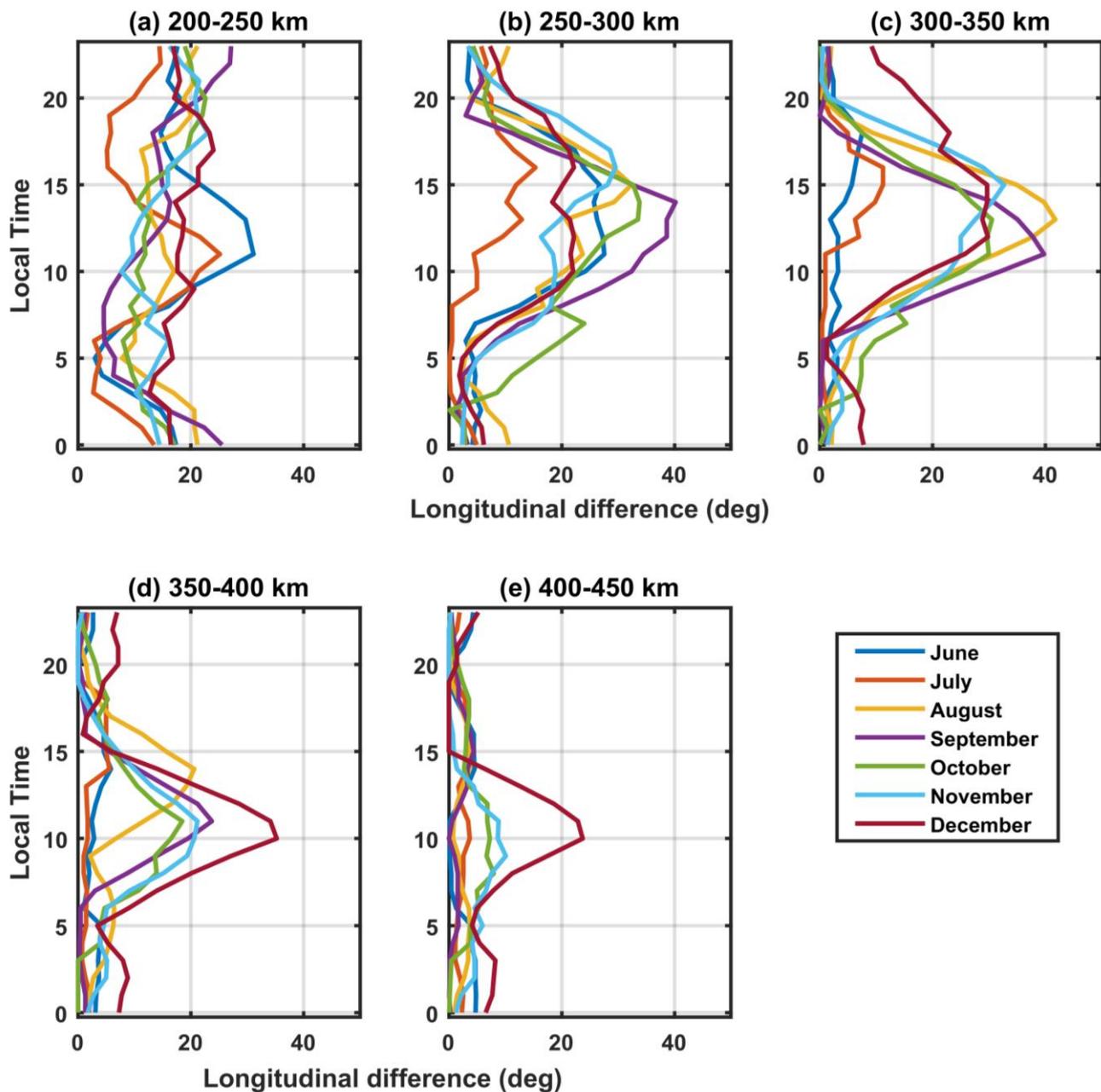**Figure 9.** (**a**–**e**) Local-time variation of the longitudinal difference between the WN4 component in the EIA crest and trough regions at 5 different altitude bands. Different months in 2020 are indicated with different colors.

4. Discussion

In this paper, the observation of longitudinal wavenumber structuring in the COSMIC-2 data in the year 2020 is presented. Wavenumber structures are visible in the local-time ionosphere in all the months of the year. The prominent wavenumber structure is the WN4 component, which is considered to be driven by the eastward-propagating nonmigrating DE3 tide. WN4 indicates eastward-propagating structures with a phase-transition node at dawn. The WN4-filtered component appears to be more complex, as it contains several different tidal modes. Earlier investigations also revealed contributions from stationary planetary waves. Luhr et al. [26] interpreted larger wavenumbers (WN2 and WN3) to also have a probable contribution by an interaction of semidiurnal migrating tides with stationary structures. Several earlier investigations focused on decomposing

the local-time ionosphere into individual tidal components, and the relative impacts of different tidal modes. The present investigation, however, deals with the vertical profile of the wavenumber structures, which has received less attention. Most of the works have utilized the ground-based TEC, satellite-derived height-averaged TEC, or other columnar measurements which give a height-integrated picture of the ionospheric density, thus limiting the investigation to a 2D analysis.

The vital aspect of the present investigation is the emphasis on the vertical profile of the longitudinal wavenumber structures, enabled by the high-rate profiling of COSMIC-2. Earlier investigations with COSMIC mostly studied the horizontal composition of the wavenumber structures, possibly due to the low rate of observations that require electron density observations over a greater altitudinal span to be averaged [6,10,11]. Longitudinal wavenumber structures were observed at all heights; however, in the altitude–longitude plane, these structures indicate tilted phase fronts. In Figure 5, the longitudinal extent of the tilted phase front in the WN4 component is of the order of the zonal wavelength of the local-time WN4 structure, i.e., ~90^0. On the other hand, the longitudinal extent of the tilted phase fronts (where seen) of the WN4-filtered component, representing lower wavenumbers, is much larger than that of the WN4 component, as can be seen in Figure 4. In addition, the tilt of the structures in the WN4-filtered component is often more than that of the WN4. This indicates that the zonal wavenumber structuring is a pan-ionospheric phenomenon having a dominant presence at all ionospheric altitudes, E-region, valley region, and F region. Vertical tilt in the phase fronts indicates that the phase of the zonal wavenumber structure varies with altitude. It is not easy to explain such an observation as the ionospheric evolution depends on multiple factors. Previous investigation using COSMIC data also indicated tilted phase fronts in WN4 with tilt observed in the height region of 200–300 km [23,24]. Above ~350 km, the tilt of the WN4 greatly reduces and the phase fronts are mostly vertical, as can be seen in Figure 5. Ionosphere F-region density is controlled by photoionization, transport due to EXB drift, neutral wind and ambipolar diffusion, and chemistry [28]. Thus, ionospheric density is not dependent on any singular driver or process. It is generally believed that the formation of EIA in the F region is controlled by the zonal electric field, and this alone cannot explain the tilted phase fronts of WN4 structures in the F region. In addition, the zonal variation of the electric field may not explain the formation of wavenumber structure at E-region heights. There can also be direct tidal impact not related to the large-scale zonal electric field. As they propagate vertically, neutral tides develop tilted phase fronts. Therefore, in the wavenumber structure (in neutral), the longitude of high/low thermospheric density will vary with height, and, accordingly, the properties of ionization production and loss will also vary with height. The wavenumber structures may be driven both by direct tidal forcing and zonal variation in the EIA formation driven by the large-scale zonal electric field. However, it is only a possible hypothesis, whose further examination is beyond the capacity of the present investigation.

The composition of WN4 can vary within the EIA belt owing to the complex electrodynamics that drives the EIA. The local-time longitude map of the WN4 component (Figure 6) indicated dissimilarities between the EIA crest and trough regions over 300 km (300–305 km bin). While the WN4 peaks in the EIA crest and trough regions were longitudinally collocated during the night time, in the daytime they are oppositely phased. In the local-time longitude map of the EIA trough region, WN4 presented a "c-shaped" propagation pattern, quite different from that over the EIA crest region. During the daytime, the "fountain effect" assists in the transport of ionospheric plasma from the Equator to the low latitudes, thus creating the "c-shaped" propagation pattern over the EIA trough region, while during the nighttime, in the absence of the "fountain effect", the WN4 peaks over the EIA crest and trough regions appear in phase. An earlier investigation by He et al. [29] studied the symmetric and antisymmetric components of the transequatorial ionospheric density structure in the context of the WN4. They reported the symmetric (antisymmetric) components to be dominant during the daytime (nighttime). Based on that, it was hypothesized that the daytime (nighttime) WN4 is driven by the zonal electric field (direct

influence of tidal winds). That study was, however, based on only a single day of observation with COSMIC utilizing only the peak density (NmF2) and peak height (HmF2) with the objective of studying the north–south asymmetry of WN4. The present study, on the other hand, focuses on the differences observed over the EIA crest and trough regions at different altitudes. Nonetheless, the present investigation seems to also corroborate the broad hypothesis of He et al. [29].

Altitudinal profiling of the WN4 over the EIA crest and trough regions reveals that the phase between the two varies with altitude. The phase also varies with the local time under consideration. The contours of the WN4 in the vertical plane (refer to Figure 7) corresponding to the EIA crest and trough regions were broadly identical during the nighttime; however, the contours appear oppositely phased during the daytime (12–13 LT). Intriguingly, the phase of the structures in the vertical plane appears to also be identical above ~400 km altitude in the daytime. Lag correlation to determine the longitudinal phase difference between WN4 over the EIA crest and trough indicates that the two are oppositely phased during the daytime below 400 km. On the other hand, the phase difference (longitudinal difference) is found to be rather less in the height region of 400–450 km both during the daytime and nighttime, except in the month of December (refer to Figure 9). However, in the month of December, the phase difference during the daytime at 400–450 km altitude is still less than those observed at lower altitude bands. It may not be simple to explain the mechanism behind such observations. One possibility is that the large-scale zonal electric field which drives the EIA actually transports the bulk plasma along/across the magnetic field line from the Equator to higher latitudes effectively only below 400 km altitude during the low solar period (as in 2020). The broad understanding is still that the formation of the WN4 structure is controlled more by the zonal electric field as the local time approaches noon, while close to midnight, WN4 structures are essentially driven by the direct action of atmospheric tides.

Note on Observational Limitation of RO Technique

In this section, observational ambiguities related to the RO technique are discussed with regard to how they are insignificant to the observational results presented in this paper. The RO technique provides an estimation of the electron density profile (E and F region) which is considered reliable [30–32]. Estimation of the true electron density profile from RO measurement has also presented challenges in the altitudes below the F1 region (e.g., [33,34]), especially in the vicinity of a sharp horizontal gradient of TEC in the EIA belt. RO-derived E-region electron density along a magnetic meridian in the EIA region has indicated 3 "pseudo peaks" (refer to Yue et al. [33]). These artificial features in the RO-derived electron density along the magnetic meridian can be attributed to the sharp horizontal gradient in the actual electron density that exists in the EIA belt. Significant artificial change in electron density is likely to occur if the plane of occultation is aligned along the magnetic meridian so that the ray path along the F region over the EIA crest passes through the valley region over the EIA trough. Such effects are highly altitude-dependent and influence electron density retrieval significantly only at lower altitudes, especially below the F1 region [33].

The observational results presented in this paper cannot be considered an artificial feature associated with ambiguity in RO-derived electron density due to the following reason(s). Firstly, the electron density was normalized (longitudinally) at every altitude bin to highlight only the relative impact of wavenumber structures at various altitudes (which also removes the ambiguity of underestimation/overestimation in absolute electron density, as normalized electron density was utilized). Secondly (and importantly), the ambiguity in electron density retrieval happens only in the meridional plane, whereas the wavenumber-4 structure is studied in the zonal plane. Yue et al. [33] also indicated a sharp deviation in electron density retrieval in the meridional direction only.

5. Conclusions

COSMIC-2 RO data were utilized to study the characteristics of longitudinal wavenumber structures of local-time electron density. Wavenumber structures were observed in all the months of 2020. The local-time propagation characteristics of WN4 revealed an eastward traverse, indicating DE3 tidal association. The unique aspect of this study is, however, related to the observation of wavenumber structure in the vertical plane enabled by high-spatial/temporal-resolution electron density profile data derived from COSMIC-2. The WN4 component indicated titled phase fronts. The main findings can be summarized as follows:

(a) The longitudinal extent of the titled phase front in the WN4 component is of the order of the longitudinal extent of the local-time wavenumber, i.e., 90^0.
(b) The WN4 structure in the F region over the EIA crest region is found to be out of phase (in phase) with respect to the EIA trough region during daytime (nighttime).
(c) Above ~400 km, the WN4 structures in the EIA crest and trough regions are seen to be in phase with each other at all local times.

The results do highlight that the formation of wavenumber structures in the local-time ionosphere is a rather complex process, not dependent on a singular driver, e.g., large-scale zonal electric field (generated by neutral winds in the E region/F region during the daytime/nighttime) or a direct propagation of nonmigrating tides.

Author Contributions: Conceptualization, L.M.J.; methodology, L.M.J. and L.-C.T.; validation, L.M.J., L.-C.T., and S.-Y.S.; investigation, L.M.J. and L.-C.T.; resources, L.M.J. and L.-C.T.; visualization, L.M.J.; project administration, L.M.J.; funding acquisition, L.M.J. All authors have read and agreed to the published version of the manuscript.

Conflicts of Interest: The authors declare no conflict of interest.

References

1. Sagawa, E.; Immel, T.J.; Frey, H.U.; Mende, S.B. Longitudinal structure of the equatorial anomaly in the nighttime ionosphere observed by IMAGE/FUV. *J. Geophys. Res.* **2005**, *110*, A11302. [CrossRef]
2. Immel, T.J.; Sagawa, E.; England, S.L.; Henderson, S.B.; Hagan, M.E.; Mende, S.B.; Frey, H.U.; Swenson, C.M.; Paxton, L.J. Control of equatorial ionospheric morphology by atmospheric tides. *Geophys. Res. Lett.* **2006**, *33*, L15108. [CrossRef]
3. England, S.L.; Maus, S.; Immel, T.J.; Mende, S.B. Longitudinal variation of the E-region electric fields caused by atmospheric tides. *Geophys. Res. Lett.* **2006**, *33*, L21105. [CrossRef]
4. Lühr, H.; Rother, M.; Häusler, K.; Alken, P.; Maus, S. The influence of nonmigrating tides on the longitudinal variation of the equatorial electrojet. *J. Geophys. Res.* **2008**, *113*, A08313. [CrossRef]
5. Fejer, B.G.; Jensen, J.W.; Su, S.-Y. Quiet time equatorial F region vertical plasma drift model derived from ROCSAT-1 observations. *J. Geophys. Res.* **2008**, *113*, A05304. [CrossRef]
6. Lin, C.H.; Wang, W.; Hagan, M.E.; Hsiao, C.C.; Immel, T.J.; Hsu, M.L.; Liu, J.Y.; Paxton, L.J.; Fang, T.W.; Liu, C.H. Plausible effect of atmospheric tides on the equatorial ionosphere observed by the FORMOSAT-3/COSMIC: Three-dimensional electron density structures. *Geophys. Res. Lett.* **2007**, *34*, L11112. [CrossRef]
7. Scherliess, L.; Thompson, D.C.; Schunk, R.W. Longitudinal variability of low-latitude total electron content: Tidal influences. *J. Geophys. Res.* **2008**, *113*, A01311. [CrossRef]
8. Wan, W.; Liu, L.; Pi, X.; Zhang, M.-L.; Ning, B.; Xiong, J.; Ding, F. Wavenumber-4 patterns of the total electron content over the low latitude ionosphere. *Geophys. Res. Lett.* **2008**, *35*, L12104. [CrossRef]
9. Pedatella, N.M.; Hagan, M.E.; Maute, A. The comparative importance of DE3, SE2, and SPW4 on the generation of wavenumber-4 longitude structures in the low-latitude ionosphere during September equinox. *Geophys. Res. Lett.* **2012**, *39*, L19108. [CrossRef]

10. Chang, L.C.; Lin, C.-H.; Yue, J.; Liu, J.-Y.; Lin, J.-T. Stationary planetary wave and nonmigrating tidal signatures in ionospheric wave 3 and wave 4 variations in 2007–2011 FORMOSAT-3/COSMIC observations. *J. Geophys. Res. Space Phys.* **2013**, *118*, 6651–6665. [CrossRef]

11. Onohara, A.N.; Batista, I.S.; Batista, P.P. Wavenumber-4 structures observed in the low-latitude ionosphere during low and high solar activity periods using FORMOSAT/COSMIC observations. *Ann. Geophys.* **2018**, *36*, 459–471. [CrossRef]

12. Maute, A.; Richmond, A.D.; Roble, R.G. Sources of low-latitude ionospheric E × B drifts and their variability. *J. Geophys. Res.* **2012**, *117*, A06312. [CrossRef]

13. Hagan, M.E.; Forbes, J.M. Migrating and nonmigrating diurnal tides in the middle and upper atmosphere excited by tropospheric latent heat release. *J. Geophys. Res.* **2002**, *107*, 4754. [CrossRef]

14. Hagan, M.E.; Forbes, J.M. Migrating and nonmigrating semidiurnal tides in the upper atmosphere excited by tropospheric latent heat release. *J. Geophys. Res.* **2003**, *108*, 1062. [CrossRef]

15. Forbes, J.M.; Russell, J.; Miyahara, S.; Zhang, X.; Palo, S.; Mlynczak, M.; Mertens, C.J.; Hagan, M.E. Troposphere-thermosphere tidal coupling as measured by the SABER instrument on TIMED during July–September 2002. *J. Geophys. Res.* **2006**, *111*, A10S06. [CrossRef]

16. Oberheide, J.; Wu, Q.; Killeen, T.L.; Hagan, M.E.; Roble, R.G. Diurnal nonmigrating tides from TIMED Doppler Interferometer wind data: Monthly climatologies and seasonal variations. *J. Geophys. Res.* **2006**, *111*, A10S03. [CrossRef]

17. Oberheide, J.; Wu, Q.; Killeen, T.L.; Hagan, M.E.; Roble, R.G. A climatology of nonmigrating semidiurnal tides from TIMED Doppler Interferometer (TIDI) wind data. *J. Atmos. Sol.—Terr. Phys.* **2007**, *69*, 2203–2218. [CrossRef]

18. Forbes, J.M.; Zhang, X.; Palo, S.; Russell, J.; Mertens, C.J.; Mlynczak, M. Tidal variability in the ionospheric dynamo region. *J. Geophys. Res.* **2008**, *113*, A02310. [CrossRef]

19. Häusler, K.; Lühr, H. Nonmigrating tidal signals in the upper thermospheric zonal wind at equatorial latitudes as observed by CHAMP. *Ann. Geophys.* **2009**, *27*, 2643–2652. [CrossRef]

20. Liu, H.; Yamamoto, M.; Lühr, H. Wave-4 pattern of the equatorial mass density anomaly: A thermospheric signature of tropical deep convection. *Geophys. Res. Lett.* **2009**, *36*, L18104. [CrossRef]

21. Jin, H.; Miyoshi, Y.; Fujiwara, H.; Shinagawa, H. Electrodynamics of the formation of ionospheric wave number 4 longitudinal structure. *J. Geophys. Res.* **2008**, *113*, A09307. [CrossRef]

22. Lei, J.; Thayer, J.P.; Wang, W.; Yue, J.; Dou, X. Nonmigrating tidal modulation of the equatorial thermosphere and ionosphere anomaly. *J. Geophys. Res. Space Phys.* **2014**, *119*, 3036–3043. [CrossRef]

23. Pancheva, D.; Miyoshi, Y.; Mukhtarov, P.; Jin, H.; Shinagawa, H.; Fujiwara, H. Global response of the ionosphere to atmospheric tides forced from below: Comparison between COSMIC measurements and simulations by atmosphere-ionosphere coupled model GAIA. *J. Geophys. Res.* **2012**, *117*, A07319. [CrossRef]

24. Pancheva, D.; Mukhtarov, P. Global Response of the Ionosphere to Atmospheric Tides Forced from Below: Recent Progress Based on Satellite Measurements. *Space Sci. Rev.* **2012**, *168*, 175–209. [CrossRef]

25. Niu, J. Relationship between wavenumber 4 pattern of sporadic E layer intensity and eastward propagating diurnal tide with zonal wavenumber 3 in low latitude region. *J. Geophys. Res. Space Phys.* **2021**, *126*, e2020JA028985. [CrossRef]

26. Lühr, H.; Rother, M.; Häusler, K.; Fejer, B.; Alken, P. Direct comparison of non-migrating tidal signatures in the electrojet, vertical plasma drift and equatorial ionization anomaly. *J. Atmos. Sol.—Terr. Phys.* **2012**, *75–76*, 31–43. [CrossRef]

27. Schreiner, W.S.; Sokolovskiy, S.V.; Rocken, C.; Hunt, D.C. Analysis and validation of GPS/MET radio occultation data in the ionosphere. *Radio Sci.* **1999**, *34*, 949–966. [CrossRef]

28. Cai, X.; Qian, L.; Wang, W.; McInerney, J.M.; Liu, H.-L.; Eastes, R.W. Hemispherically asymmetric evolution of nighttime ionospheric equatorial ionization anomaly in the American longitude sector. *J. Geophys. Res. Space Phys.* **2022**, *127*, e2022JA030706. [CrossRef]

29. He, M.; Liu, L.; Wan, W.; Wei, Y. Strong evidence for couplings between the ionospheric wave-4 structure and atmospheric tides. *Geophys. Res. Lett.* **2011**, *38*, L14101. [CrossRef]

30. Syndergaard, S. A new algorithm for retrieving GPS radio occultation total electron content. *Geophys. Res. Lett.* **2002**, *29*, 55-1–55-4. [CrossRef]

31. Nicolls, M.J.; Rodrigues, F.S.; Bust, G.S.; Chau, J.L. Estimating E region density profiles from radio occultation measurements assisted by IDA4D. *J. Geophys. Res.* **2009**, *114*, A10316. [CrossRef]

32. Wu, D.L. New global electron density observations from GPS-RO in the D- and E-Region ionosphere. *J. Atmos. Sol.—Terr. Phys.* **2018**, *171*, 36–59. [CrossRef]

33. Yue, X.; Schreiner, W.S.; Lei, J.; Sokolovskiy, S.V.; Rocken, C.; Hunt, D.C.; Kuo, Y.-H. Error analysis of Abel retrieved electron density profiles from radio occultation measurements. *Ann. Geophys.* **2010**, *28*, 217–222. [CrossRef]

34. Wu, K.; Su, C.; Chu, Y. Improvement of GPS radio occultation retrieval error of E region electron density: COSMIC measurement and IRI model simulation. *J. Geophys. Res. Space Phys.* **2015**, *120*, 2299–2315. [CrossRef]